Final Report

for the period

UCRL--15926

DE87 013494

1 October 1985 - 30 September 1986

Rayleigh-Taylor Instability in Compressible Fluids

Principal Investigator: B. Sturtevant

Graduate Aeronautical Laboratories

California Institute of Technology

Pasadena, CA 91125

Prepared for the

U.S. Department of Energy

Division of Energy Technology

Subcontract 7961805 under DOE W-7405-ENG-48

October 7, 1986

DISCLAIMER

Work performed under the auspices of the U.S. Department of Energy by Lawrence Livermore National Laboratory under contract number W-7405-ENG-48.

Rayleigh-Taylor Instability in Compressible Fluids

1. Introduction

The purpose of this research program is to:

"investigate fluid dynamic instabilities and mixing initiated by the interaction of shock waves with interfaces between light and heavy gases. In particular, the nonlinear stage of shock-initiated Rayleigh-Taylor instability (also known as the Richtmeyer-Meshkov instability), the secondary instabilities (e.g., the Kelvin-Helmholtz instability) arising therefrom and the resulting mixing of the two gases are of interest".

In this report we describe activities during the performance period 1 October 1985 to 30 September 1986. The report is in two sections. In the first, we report on the design and construction of a test section for the vertical shock tube facility in which continuous interfaces between two gases of different density can be arranged for subsequent impulsive acceleration by shock waves. In addition, we describe the control system for the vertical shock tube facility that has been installed during the past year.

In the second section we report on a series of experiments investigating the shock-induced growth of long-wavelength perturbations on plane interfaces oriented normal to the direction of shock propagation which was carried out in 1984 but was only reported briefly in the proposal of 9 August, 1984. The experiments were of a preliminary nature and there were large uncertainties in the initial shape of the interface prior to shock acceleration. Nevertheless, we present the results in some detail and include more shadowphotographs to illustrate the growth of perturbations on the interface. Observed absolute and relative growth rates are

presented in tabular form, and comparison is made with the classical linear theory for shock-induced Rayleigh-Taylor instability. The discrepancy between measurement and theory is large, well outside the uncertainties in the initial static deflection of the interface. Thus we are forced to conclude that, after passage of the shock, the membrane (and the interface) stretched substantially before detaching from the point at which it was clamped. If correct, this observation has important implications about past and future experiments. It should be confirmed by careful experimentation at the earliest possible date.

2. Test Section and Control System

During the current year the entire effort has been expended in an attempt to accomplish the completion of the vertical shock tube facility. In particular, as proposed for this period, a test section was designed and built. The design of the test section was driven by the requirement that a continuous interface of from millimeters to centimeters thickness between heavy gas at the bottom and light gas above be set up in the neighborhood of the observing windows before arrival of the shock. Thus the test section incorporates an automatic system for withdrawal of a thin horizontal metal sheet separating the light and heavy gases seconds before a run. Rather than use an existing section of the shock tube originally intended for use with discontinuous interfaces, the design study showed that, in order to set up continuous interfaces, it was necessary to fabricate the section from aluminum plate, fastened by dip brazing. Heavier gauge material was required to withstand the design internal pressure of 300 psi in the presence of access holes on three out of four sides of the test section required for the two viewing windows and for the sliding metal sheet at two stations.

Figure 2.1 is a photograph of the finished product, including the metal sheet installed at the window station and the structure for supporting and withdrawing it. The aluminum from which the test section is made

is anodized black. The ball screw and bearing visible at the top are used to drive the plate, shown in a semi-retracted position. The stepping motor which powers the ball screw to withdraw the plate at up to 30 cm/s is not shown. Figure 2.2 shows an exploded view of the support structure for the metal plate at the test section wall, a portion of the apparatus obscured in Figure 2.1. The Lucite block fits into the access hole in the test section wall and acts as a guide, while the metal assembly houses screws to adjust the location of the plate. As can easily be seen from the photographs, the test section is a major machining nightmare. Indeed, its fabrication was the major cause for delay during the current year. Had we proceeded with the original plan to use a short length of the shock tube material for the test section, we would likely by now have acquired some photographs in experiments similar to those reported below, but, in the long run, the acquisition of data from a variety of well-defined, easily-controlled experiments would have been delayed. The test section that was ultimately built will be useful for experiments with both continuous, membrane-free interfaces and discontinuous interfaces formed by thin plastic membranes.

In recent hydrotests of the pressure-holding capacity of the test section it was possible to achieve only 100 psi before two small leaks became evident in the dip-brazed joints where the outside surface had subsequently been machined. It is well known that machining can open up voids in dip brazed joints, but it was not expected that open channels would occur all the way through the 2 inch thick joints. Attempts are still underway to find a method for plugging the holes.

Installation of the controls for operating the shock tube is essentially complete. Control panels have been erected at both the driver tube level and at the test section level. The panels contain pressure gauges and valves necessary for filling the driver and driven sections. Because the shock tube extends through three stories of the Guggenheim Laboratory, the operations require remote pressure sensing and readout and electronic valve actuation at both the test section and driver section stations. The

facility is arranged so that in setting up for a run, the diaphragm is changed and the system pumped by an operator at the driver level (presently at the top of the facility), while all the gas filling operations are controlled at the test section level. In this way, for some configurations in which deformation of the shock tube diaphragm during filling may be a critical factor, the gas flows can be carefully sequenced. To control the gas filling of the driven and test sections, a feedback system has been designed and built. It uses a differential pressure transducer to ensure that both sides of the sliding plate (or membrane) are always at the same pressure to avoid leaks across the plate and undesired plate deflection. The electronics necessary to control the experiment have been designed and built. They consist of two adjustable delay/pulse-width boxes to operate the spark light source for the schlieren system and the camera shutter, an interface box for the differential pressure transducer, and the pressure feedback system circuitry.

A "boost tank" which can withstand 2000 psi has been installed between the driver gas bottle farm and the driver section. It is connected to the driver section by a short, large-diameter line and solenoid valve. Rapid release of gas from the boost tank into the driver section will be used to bring the driver pressure from just below the breaking pressure of the diaphragm to the rupture pressure, thus acting in place of a rupturing tool or plunger. Control of the instant at which the experiment occurs is required for the continuous membrane-free interface experiments, because timing of shock arrival after withdrawal of the metal dividing plate is critical.

The parts for the optical system for flow visualization have been fabricated but not assembled. The tables that support the optical components have been built and installed at the test-section level. Mirrors (8 in dia, 60 in focal length) for the schlieren system have been purchased and the adjustable mirror mounts have been built and anodized.

3. Shock-Induced Rayleigh-Taylor Instability of Normal Interfaces

The experiments described in this section were performed in the horizontal 15 cm dia shock tube at GALCIT. An 8.9 cm square 120 cm long test section was fitted to the end of the shock tube and was matched to the circular cross section of the basic facility with a 1.8 m long 'cookie-cutter' extension mounted inside the tube. The motion of wave fronts and interfaces was recorded with a spark shadowgraph optical system through 15 cm dia windows. The field of view in the photographs presented here is approximately 95 mm by 73 mm.

An interface between heavy and light gases was set up at a location 12 cm upstream of the viewing window (cf. Figures 3.3 ff. for schematic views of the arrangement) by clamping a thin cellulose membrane between two sections of the square test section. In this way it was insured that the interface extended across the entire width of the test section free of obstruction and that the walls were smooth, but it was impossible to measure the configuration of the membrane accurately. The initial deflection of the membrane was adjusted to a neutral, minimum-deflection position or to a nominal upstream- or downstream-deflected state by controlling a slight differential pressure between the light and heavy gases. With a simple clamped membrane the effective wavelength of the initial perturbation was twice the height of the shock tube. Shorter wave perturbations were arranged by stretching fine wires across the test section on the side of the membrane toward which it was to be deformed. In one case (Figure 3.4 bottom) wires were stretched both horizontally and vertically across the middle of the shock tube in a crossed-wire configuration. The initial deflection η_0 of the membrane was estimated to be approximately 1, 3, 2, 1, or 1.5 mm, depending on whether the configuration was the neutral, single-wave, 2-wave, 4-wave or crossed-wire arrangement, respectively.

Figures 3.1 - 3.10 and tables 1 - 5 summarize the results. The times quoted therein refer to the time from shock arrival at the undeflected membrane location to the time of the photograph. The tables give the

deformation of the interface in mm, measured from the photographs, and also the same quantity normalized by the (known) half wavelength of the initial perturbation ($\lambda/2$) and by its (estimated) amplitude (η_0). η_1 is a corrected post-shock amplitude which accounts for the compression by the normal interaction of an incident plane shock wave with an interface between the gas pair in question. Note that this is not the same as the less accurate correction used by Meshkov, namely, the compression by an incident shock in the pure upstream gas. Normalizing with the perturbation wavelength is expected to be appropriate for late-time saturated growth, when the initial conditions have been "forgotten". The fact that the results presented in the tables in such a form do not scale in any consistent fashion, while those normalized with initial amplitude do, confirms that all of the experiments reported here are "early time" experiments.

Figures 3.1 and 3.2 and Table 1 show the behavior of air accelerated into a mixture of argon and helium having the same density and sound speed as air but a different index of refraction, so the interface is rendered visible to the shadowgraph system. The initial position and configuration of the membrane relative to the viewing window are shown schematically in later figures. The table shows that the observed deflections are a factor of 3 - 5 larger than the estimated initial amplitudes, while, according to instability theory, the growth should be extremely slight. As we shall see, this discrepancy is typical of all of the measurements reported here.

Figures 3.3 and 3.4 show an air/helium interface after about 950 μs of growth. The air/helium interface is Rayleigh-Taylor stable, so the initial distortion flattens and then overshoots in the opposite direction. The familiar bubble and spike configuration of the Rayleigh-Taylor instability is readily seen in the figures. There is substantial evidence of vorticity present in the pictures of the spikes, including the familiar hammerhead configuration, in figures 3.3 bottom, and 3.4 top and bottom. The seventh column of Table 2 shows that, based on the initial estimated deformation, the growth has been very large, from 3 - 9 times the

predicted growth.

In figures 3.5 and 3.6 time sequences are shown of the development of the configurations shown in figure 3.3 bottom and 3.4 bottom, respectively, after the shock wave, which reflects from the shock tube endwall, returns and decelerates the interface. Since this configuration is now Rayleigh-Taylor unstable, subsequent growth and distortion are both expected and observed.

Figures 3.7 - 3.10 and Tables 4 and 5 give a similar sequence of data for the initially unstable configuration Air/R22 (R22 has molecular weight 86.5 and standard density 4.72 kg/m^3), except in this case figure 3.8 bottom is not for the crossed-wire configuration as was the analogous picture in figure 3.4 bottom. Here the observations imply a growth rate, based on the estimated initial deformation, of from 30% greater than theoretical for the harmonic cases to 7 times greater for the fundamental, suggesting that perhaps the membrane does not stretch as much during shock impact when backed by R22 as when backed by helium. The interaction of the R22 interface with the reflected wave (figures 3.9 and 3.10), being a stable configuration, causes reversal of the distorted interface. Consequently, for intermediate times the deformation of the interface is not monatonic, so two extremes are cited in Table 5.

We believe that the discrepancies between theory and experiment cited above can be attributed to poor definition of the initial deflection of the interface, due to the impossibility of obtaining measurements at the instant of shock impingement. The membrane material used in these experiments is a formulation for indoor model airplanes and is rather elastic. Indeed, it was chosen for this property, which makes it easy to work. The maximum stretch of the membrane can be estimated by equating the time during which stretching occurs at the shock-induced velocity of the interface with the time required for a tear to propagate across the membrane (say, for 9 cm) at the Culick velocity,

$$V_c = \left(\frac{2\sigma}{\delta\rho}\right)^{1/2} ,$$

where σ is the surface tension of the film, δ is its thickness, and ρ is the density of the film material. Taking reasonable values for the film properties (δ = 0.56 μm, ρ = 1100 kg/m^3, $\sigma \approx$ 1 N/m), we get $V_c \approx$ 50 m/s. Thus, the maximum stretch possible at 150 m/s is about 30mm, very close to the value required to make Case 9, the worst case in Table 2, agree with the prediction of linear stability theory. We conclude that significant stretch occurs before membrane failure and that it is very important that post-shock-impingement deflections be measured in studies with discontinuous interfaces supported by membranes.

TABLE 1.
He/Ar Mixture <| Air
$M_s = 1.2$

Run	Figure	Time (μs)	η_0 (mm) (approx)	η (mm)	$\frac{\eta}{\lambda/2}$	$\frac{\eta}{\eta_1}$	$\frac{\eta}{\eta_0}$	$\left\lvert\frac{\eta}{\eta_1}\right\rvert_{\text{theor}}$
1. Fundamental	3.1 top	1977	3	8.5	0.094	3.4	2.8	0.94
2. Fundamental	3.1 middle	1981	-1	-5.0	-0.056	6.0	5.0	1.02
3. Fundamental	3.1 bottom	1981	-3	-12.0	-0.133	4.8	4.0	1.02
4. 4^{th} Harmonic	3.2 top	1974	1	3.0	0.133	3.6	3.0	0.90
5. 2^{nd} Harmonic	3.2 middle	1983	2	7.3	0.162	4.5	3.7	0.95
6. 2^{nd} Harmonic	3.2 bottom	1984	-2	-6.0	-0.178	4.8	4.0	0.95

NOTE: $\frac{\eta_1}{\eta_0} = 0.77$

TABLE 2.
He <| Air
$M_s = 1.2$

Run	Figure	Time (μs)	η_0 (mm) (approx)	η (mm)	$\frac{\eta}{\lambda/2}$	$\frac{\eta}{\eta_1}$	$\frac{\eta}{\eta_0}$	$\left\lvert\frac{\eta}{\eta_1}\right\rvert_{\text{theor}}$
7. Fundamental	3.3 top	961	3	-48	-0.53	-18.8-16		-2.7
8. Fundamental	3.3 middle	959	1	-18	-0.20	-21.2-18		-2.7
9. Fundamental	3.3 bottom	928	-3	60	0.67	-23.5-20		-2.6
10. 4^{th} Harmonic	3.4 top	950	-1	30	1.33	-35.3-30		-13.6
11. 2^{nd} Harmonic	3.4 middle	961	2	-39	-0.86	-21.2-18		-6.5
12. 2^{nd} Harmonic Crossed Wires	3.4 bottom	957	-1.5	46	1.02	-36.1-30.6		-6.3

NOTE: $\frac{\eta_1}{\eta_0} = 0.87$

TABLE 3.
He <| Air
EFFECT OF REFLECTED WAVE
$M_s = 1.2$

Run	Figure	Time (μs)	η_0 (mm) (approx)	η (mm)	$\frac{\eta}{\lambda/2}$	$\frac{\eta}{\eta_1}$	$\frac{\eta}{\eta_0}$
13. Fundamental	3.5 top	969	-3	63	0.70	-24.7	-21.0
14. Fundamental	3.5 middle	1083	-3	79	0.88	-30.9	-26.3
15. Fundamental	3.5 bottom	1220	-3	92	1.02	-36.1	-30.7
16. 2nd Harmonic	3.6 top	958	-2	38	0.84	-22.4	-19.0
17. 2nd Harmonic	3.6 middle	1229	-2	71	1.58	-41.8	-35.5
18. 2nd Harmonic	3.6 bottom	1531	-2	100?	2.2	-58	-50

NOTE: $\frac{\eta_1}{\eta_0} = 0.85$

TABLE 4.
R22 <| Air
$M_s = 1.2$

Run	Figure	Time (μs)	η_0 (mm) (approx)	η (mm)	$\frac{\eta}{\lambda/2}$	$\frac{\eta}{\eta_1}$	$\frac{\eta}{\eta_0}$	$\left\{\frac{\eta}{\eta_1}\right\}$ theor
19. Fundamental	3.7 top	2212	3	48	0.53	23.2	16	4.6
20. Fundamental	3.7 middle	2425	1	11	0.12	15.9	11	4.9
21. Fundamental	3.7 bottom	2195	-3	-70	0.78	33.8	23.3	4.5
22. 4th Harmonic	3.8 top	2432	1	15	0.67	21.7	15	16.7
23. 2nd Harmonic	3.8 middle	2492	2	16	0.36	11.6	8	9.1
24. 2nd Harmonic	3.8 bottom	2422	-2	-23	-0.51	16.7	11.5	8.8

NOTE: $\frac{\eta_1}{\eta_0} = 0.69$

TABLE 5.
R22 <+ Air
EFFECT OF REFLECTED WAVE

$M_s = 1.2$

Run	Figure	Time (μs)	η_0 (mm) (approx)	η (mm)	$\frac{\eta}{\lambda/2}$	$\frac{\eta}{\eta_1}$	$\frac{\eta}{\eta_0}$
25. Fundamental	3.9 top	2312	3	35	0.39	16.9	11.7
26. Fundamental	3.9 middle	2511	3	32	0.36	15.5	10.7
27. Fundamental	3.9 bottom	2979	3	12	0.13	5.8	4.0
28. Fundamental	3.10 top	3003	3	-16	-0.18	-7.7	-5.3
				10	0.11	4.8	3.3
29. Fundamental	3.10 middle	3510	3	-44	-0.49	-21.3	-14.7
				8	0.09	3.9	2.7
30. Fundamental	3.10 bottom	4008	3	-72	-0.8	-34.8	-24
				4	0.05	1.8	1.4

NOTE: $\frac{\eta_1}{\eta_0} = 0.69$

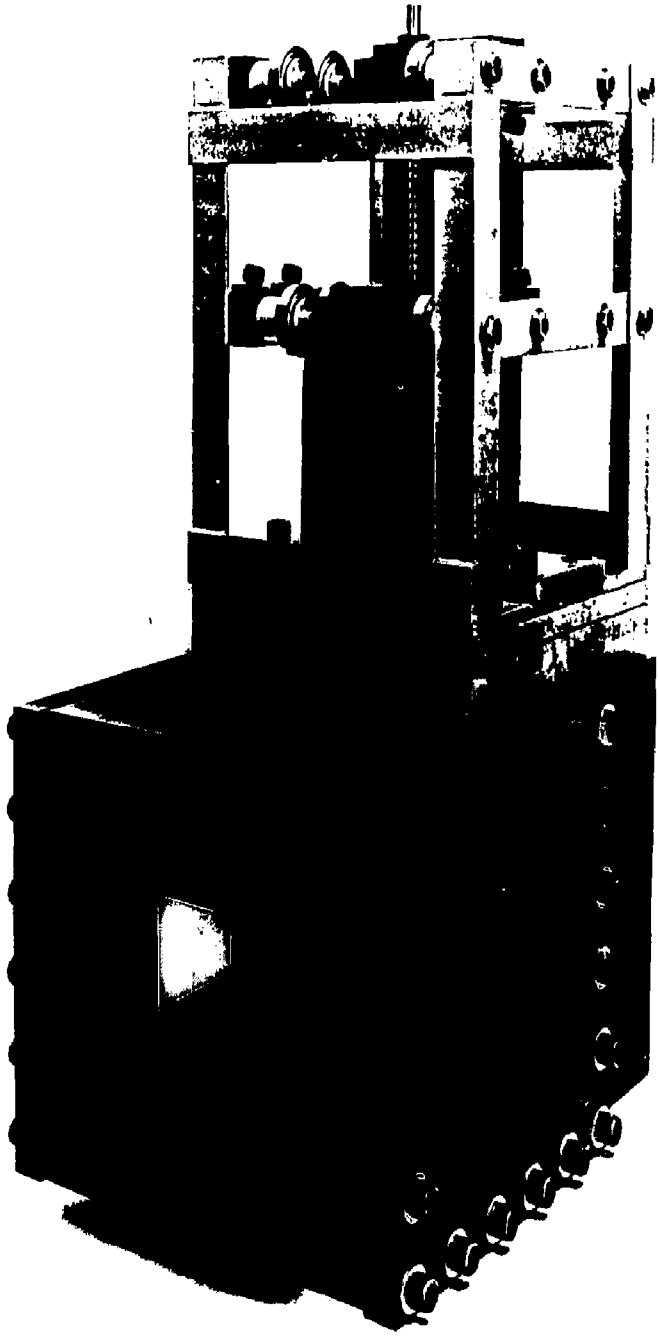

Figure 2.1

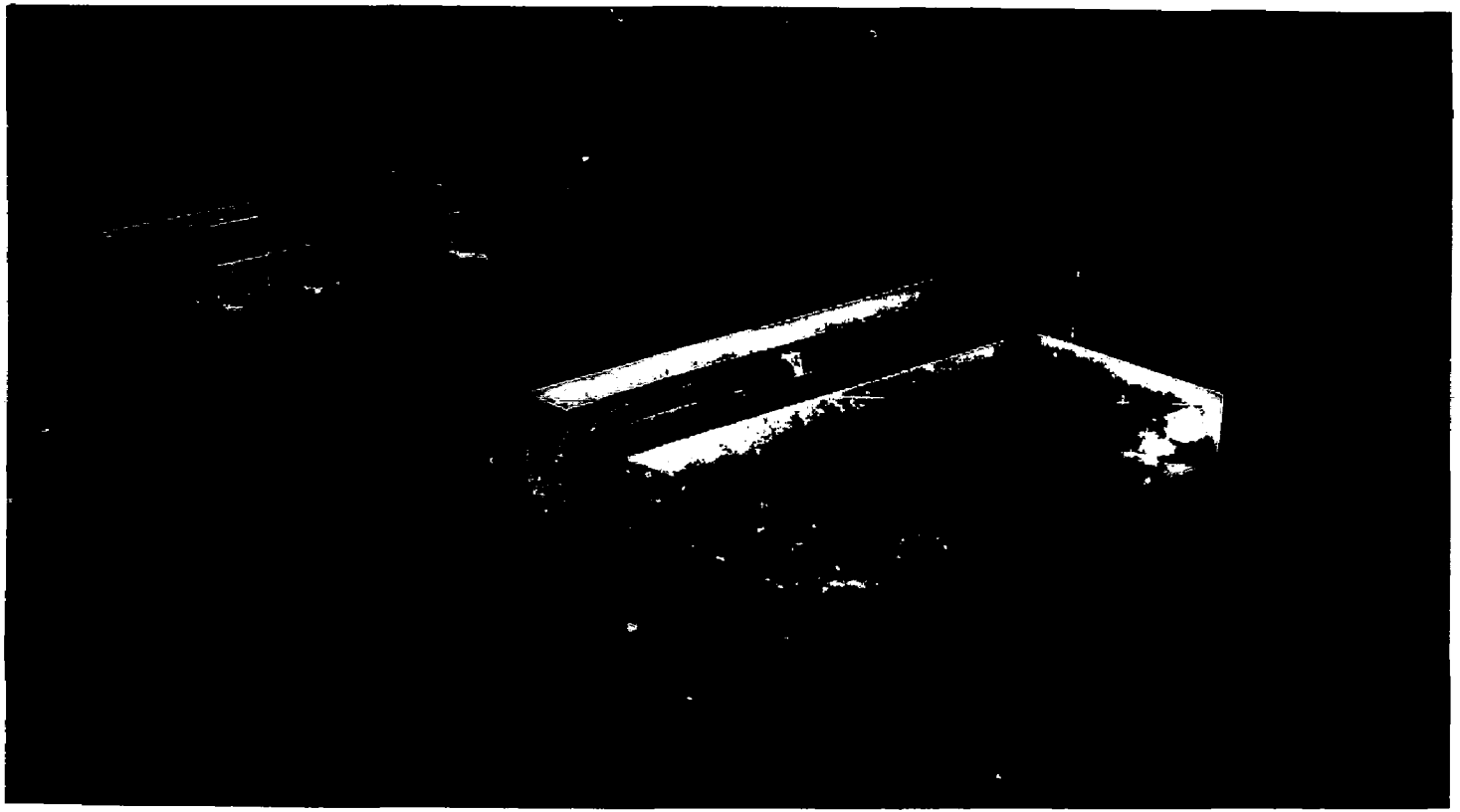

Figure 2.2

1/3 Helium-2/3 Argon | Air A=-0.0035 ← | M_s=1.2

Fondamental Mode

Figure 3.1

1/3 Helium-2/3 Argon | Air A=-0.0035 ←| M_S=1.2

Harmonics

t=1973 μs

t=1983 μs

t=1984 μs

Figure 3.2

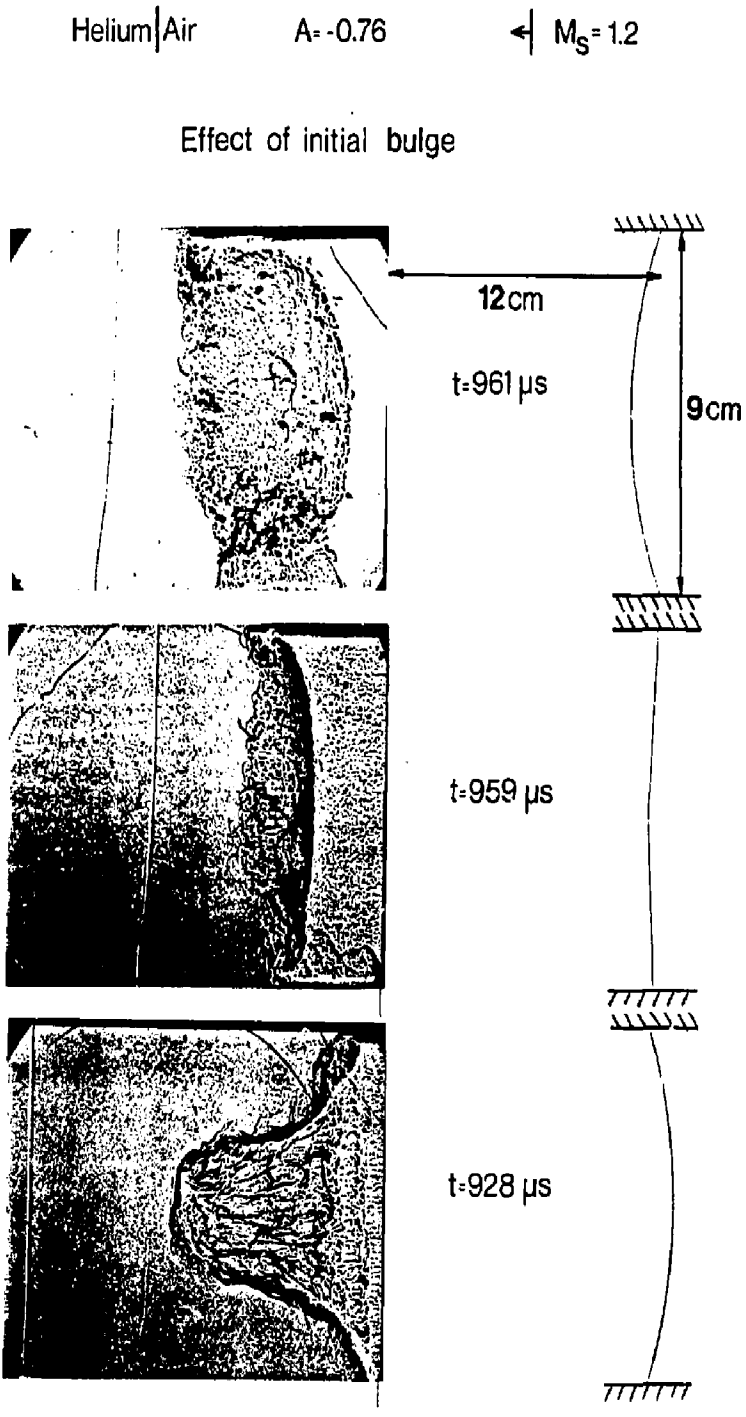
Helium|Air
A= -0.76
M_S= 1.2
Effect of initial bulge
12cm
t=961 μs
9cm
t=959 μs
t=928 μs

Figure 3.3

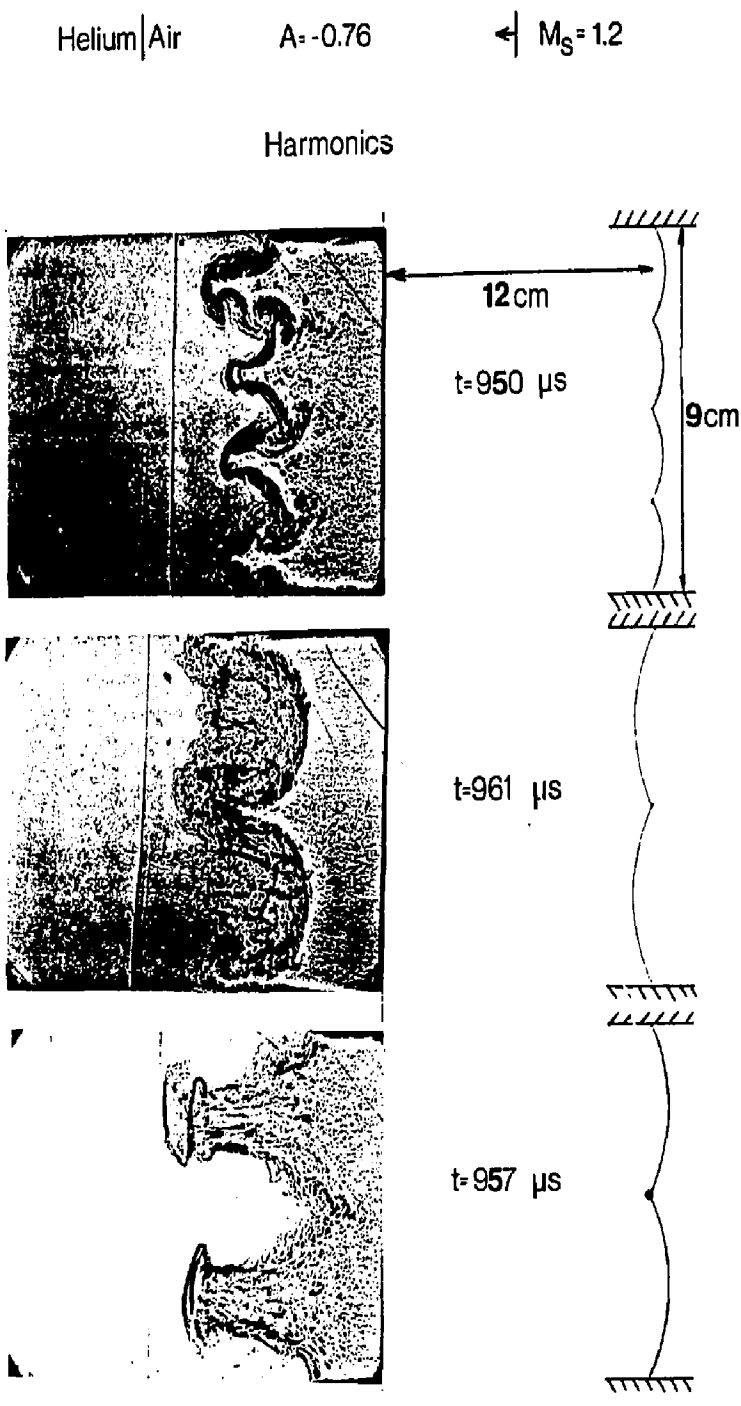
Helium | Air
A= -0.76
M_S = 1.2
Harmonics
12 cm
t=950 μs
9cm
t=961 μs
t=957 μs

Figure 3.4

Helium | Air A = -0.76 ⟵| M_s = 1.2

Effect of reflected wave on fundamental

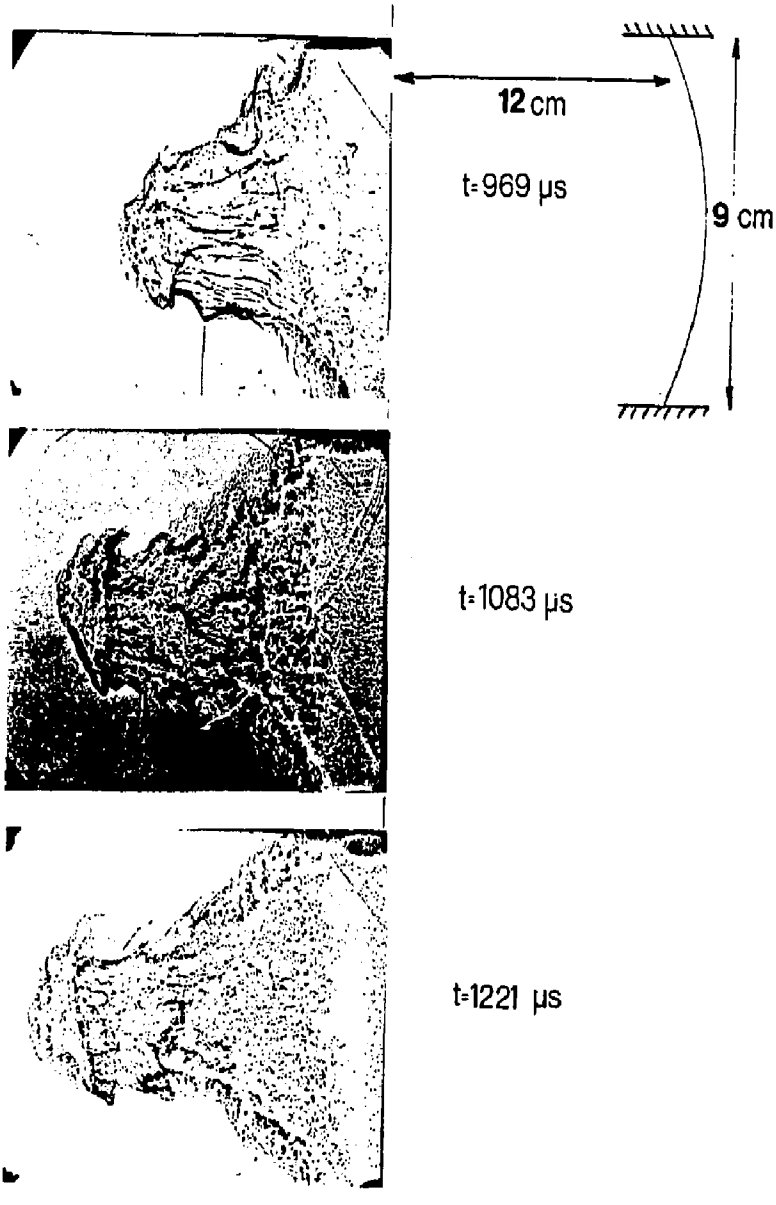

Figure 3.5

Helium | Air A= -0.76 ← | M_s = 1.2

Effect of reflected wave on second harmonic

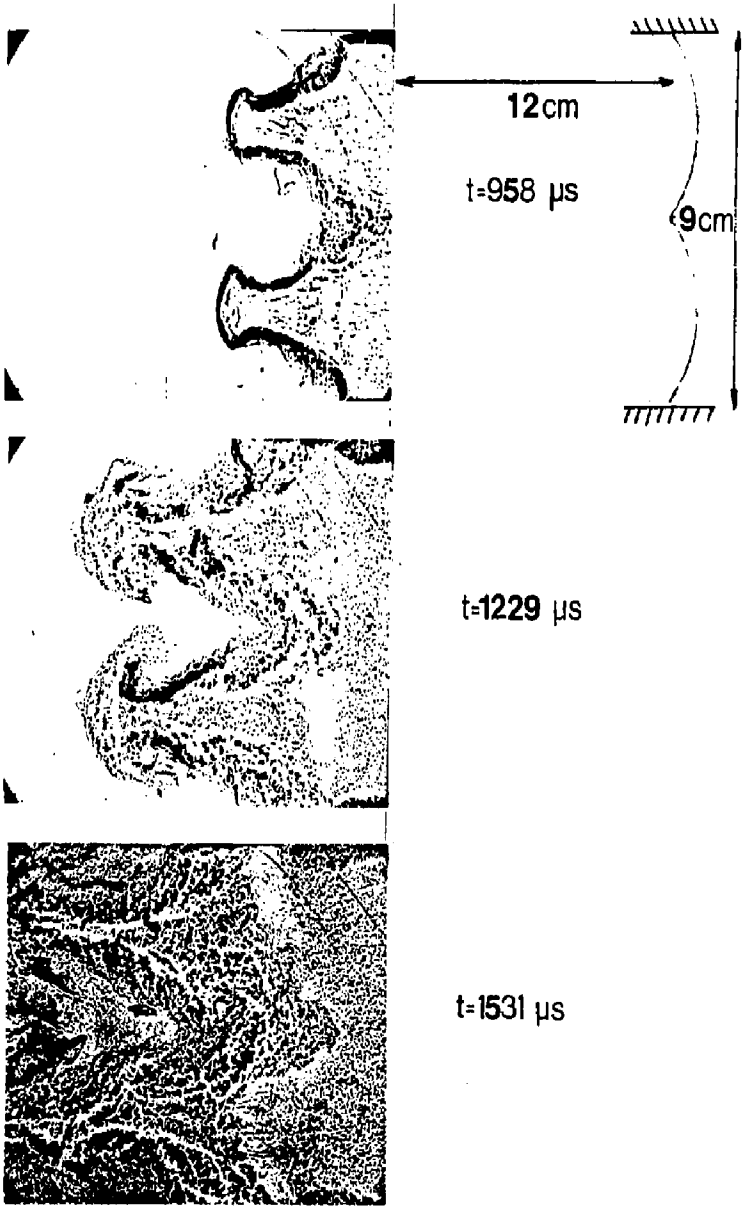

Figure 3.6

Freon (R_{22}) | Air A=0.57 ◀| M_s=1.2

Effect of initial bulge

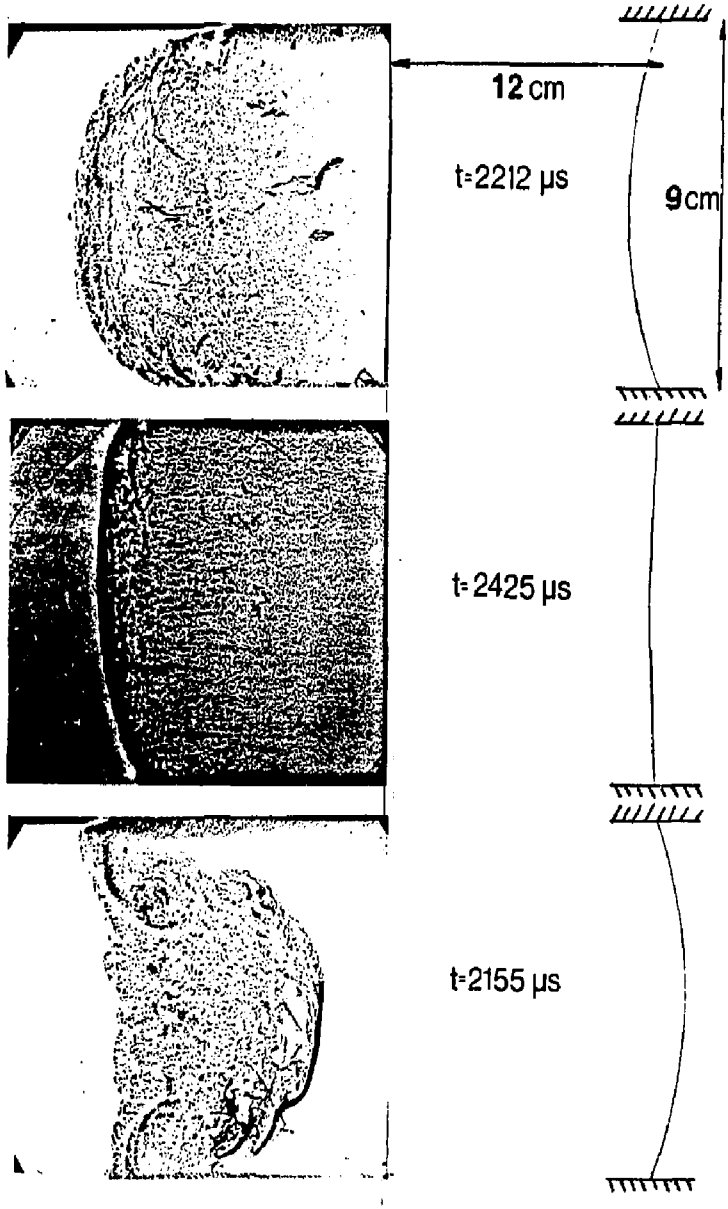

Figure 3.7

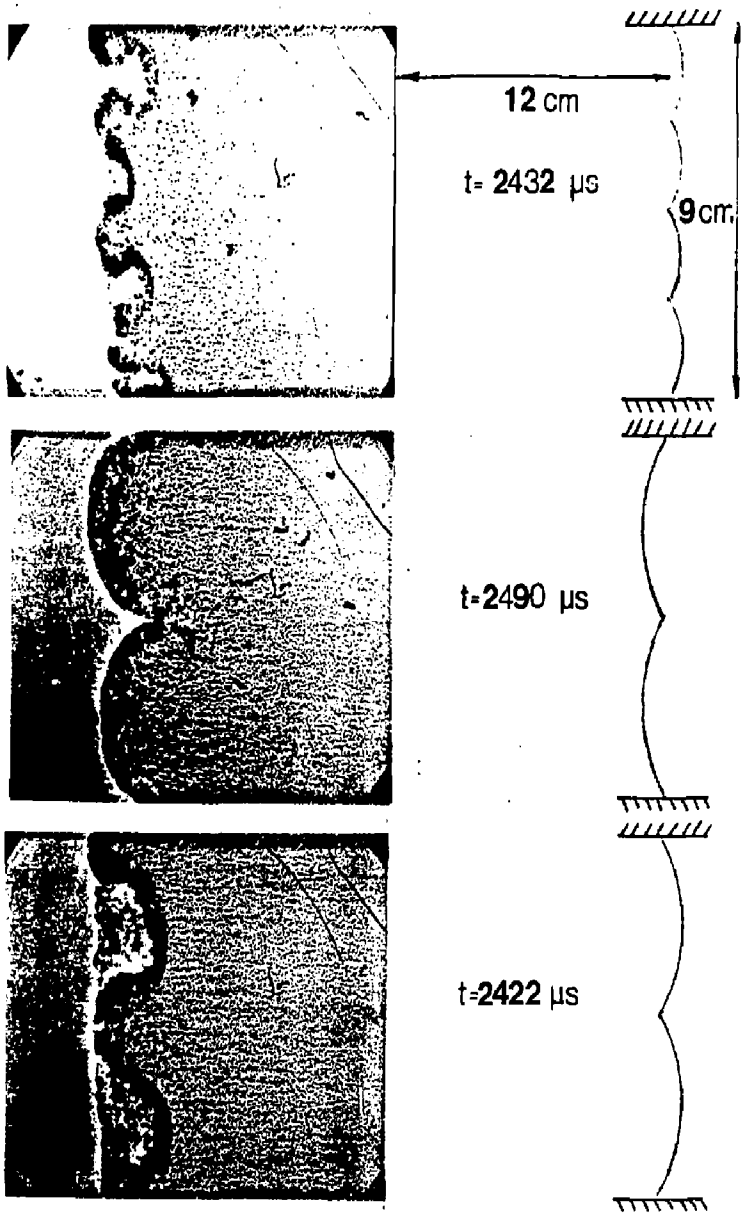
Freon (R_{22}) | Air A=0.57 ◄| M_s=1.2
Harmonics
12 cm
t= 2432 μs
9 cm
t=2490 μs
t=2422 μs

Figure 3.8

Freon (R_{22}) | Air A=0.57 ◄| M_s=1.2

Effect of reflected wave on fundamental

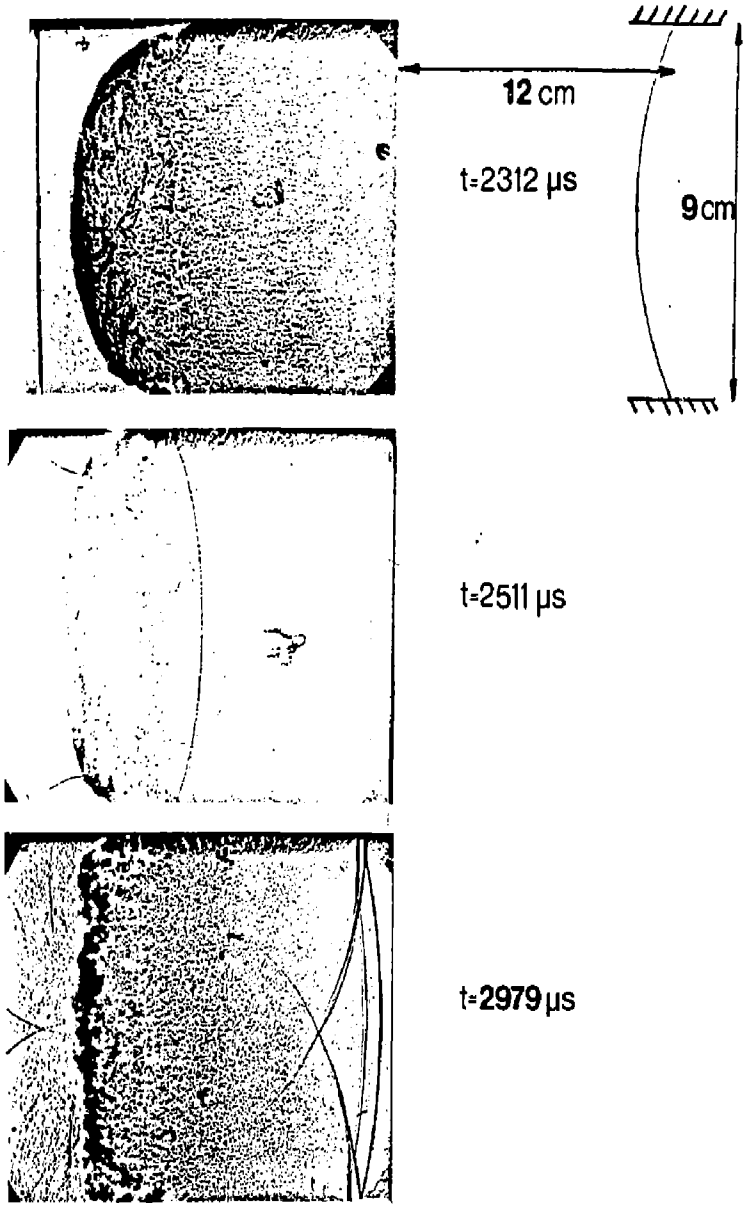

Figure 3.9

Freon (R_{22}) | Air A=0.57 ← | M_s=1.2

Effect of reflected wave on fundamental

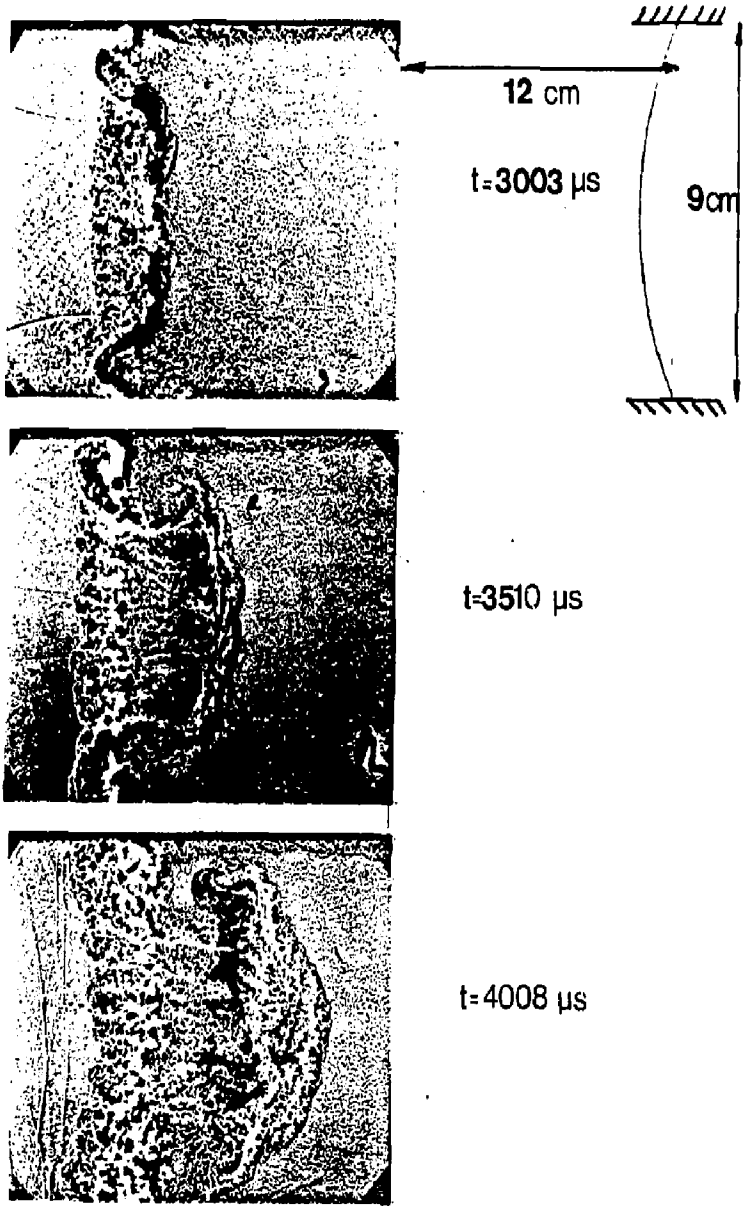

Figure 3.10